# Recovering local shape of a mirror surface from reflection of a regular grid

Silvio Savarese[1], Min Chen[2], and Pietro Perona[1]

[1] California Institute of Technology, Mail stop 136-93, Pasadena, CA 91125, USA
{savarese,perona}@vision.caltech.edu,
WWW home page: http://www.vision.caltech.edu/
[2] Oracle Parkway, Redwood City, CA 94065, USA
{min.chen}@oracle.com

**Abstract.** We present a new technique to recover the shape of an unknown smooth specular surface from a single image. A calibrated camera faces a specular surface reflecting a calibrated scene (for instance a checkerboard or grid pattern). The mapping from the scene pattern to its reflected distorted image in the camera changes the local geometrical structure of the scene pattern. We show that if measurements of both local orientation and scale of the distorted scene in the image plane are available, this mapping can be inverted. Specifically, we prove that surface position and shape up to third order can be derived as a function of such local measurements when two orientations are available at the same point (e.g. a corner). Our results generalize previous work [1, 2] where the mirror surface geometry was recovered only up to first order from at least three intersecting lines. We validate our theoretical results with both numerical simulations and experiments with real surfaces.

## 1 Introduction and Motivation

Shiny surfaces have traditionally been considered a nuisance in computer vision. Many objects of interest and man-made surfaces are smooth and shiny, such as a metal spoon or a clean automobile, and violate the hypothesis of traditional shape reconstruction techniques (e.g. shape from shading, texture gradient, etc...). In fact, it is not possible to observe the intrinsic surface of a mirror but only what is reflecting. This additional cue, however, may be precisely exploited in order to infer the shape of this category of objects.

In this paper we present a new technique to recover local shape of an unknown smooth specular surface by observing the deformation of the reflection of a regular pattern in a calibrated scene (for instance, a checkerboard grid), using a calibrated camera (see Fig. 1). Our approach extends and generalizes our previous work [1–3] based on a novel observation that the mapping from the scene grid to the reflected curved grid in the camera image plane due to mirror reflection not only changes the "orientation" of the grid lines but also "stretches" the grid step, modifying the local scale of the pattern. Such a deforming mapping can be easily illustrated by the grid points $(1, 2, 3, 4, 5)$ and

their corresponding points $(1', 2', 3', 4', 5')$ in the curved grid reflected on the mirror surface shown in Fig 1. We first analyze this map and derive analytical expressions for the local geometry in the image (namely, first- and second-order derivatives at the intersection points of the curved grid) as a function of mirror surface position and shape. We then study the inverse problem and derive surface position and shape up to third order as a function of local position, orientation and local scale measurements in the image when two orientations are available at the same point. Such local measurements may be computed at a point (e.g. $1'$ in Fig. 1(c)) from its four neighboring reflected points (e.g. $2', 3', 4', 5'$). By comparing these measurements with their corresponding analytical expressions, we induce a set of constraints, which lead to solutions for surface position, as well as closed-form solutions for normal, curvature and third-order local parameters of the surface around the reflected point of interest. As a result, our reconstruction approach is only "technically" sparse as we can estimate local shape (i.e. surface orientation, curvature and third order parameters) in the neighborhood of each reflected point. In other words, we obtain a "piece-wise parabolic" reconstruction, where each "piece" is a vertex of a paraboloid. A robust estimation of the surface's shape may be ultimately obtained by integrating such information.

### 1.1 Previous Work and Paper Organization

Pioneering work on specular surfaces reconstruction was carried out by Koenderink [12], Blake [6, 5] and Zisserman [15] who tackled the problem under the hypothesis of viewer motion. Other approaches include those based on mathematical models of specular reflections [10, 11], analyzing 3D surface profiles travelled by virtual features (Oren and Nayar [13]), as well as their extensions [14]. Halsead et al. [9] proposed a reconstruction algorithm where a surface global model is fitted to a set of normals obtained by imaging a pattern of light reflected by specular surface. Their results were applied to interactive visualization of the cornea. Perard [16] and Tarini *et al.* [17] proposed a structured lighting technique for the iterative reconstruction of surface normal vectors and topography. Bonfort *et al.* [18] presented a voxel-based approach in the spirit of multiple view (space carving) algorithms. Among these techniques, some limitations are the necessity of having available a certain degree of knowledge on shape and position of the object; multiple images under different condition of the illuminant; dedicated hardware equipment. Savarese *et al.* [1–3] tried to overcome the above limitations and tackled the monocular single-image case using a local and differential approach: local measurements of position and orientation of three intersecting lines were used to recover first-order surface geometry (and second-order up to one free parameter). By exploiting measurements of both local scale and orientation, our work generalizes and extends this result to be able to recover the local surface geometry up to third-order accuracy using fewer lines. Table 1 summarizes the difference between our results and previous work [2, 3].

The rest of the paper is organized as follows. After introducing the problem formulation in Section 2, we present in Section 3 full analytical expressions for

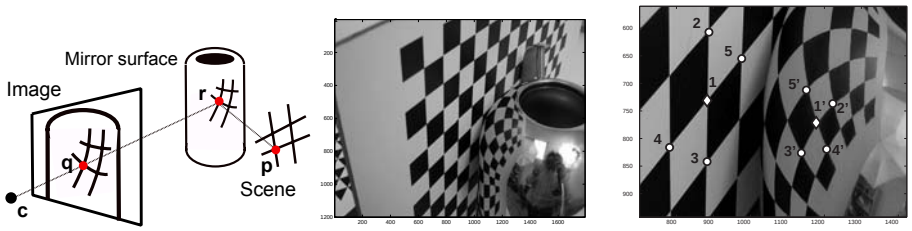


(a) (b) (c)

**Fig. 1. Setup**. (a) A camera is facing a specular surface reflecting a scene. (b) Image seen from the camera. (c) Points correspondence $(1, 2, 3, 4, 5)$ and $(1', 2', 3', 4', 5')$ under reflection.

the first- and second-order derivatives of a reflected image curve, and then derive closed-form solutions for the unknown surface parameters in Section 4. In Section 5, we describe how to measure derivatives of a reflected image curve using numerical approximation and address its associated error issues. We finally validate our theoretical results with both numerical simulations and experiments with real surfaces in Section 6.

**Table 1.** Comparison of our results with previous work

| **Method** | **Measurements** | **Estim. surface quantities** |
|---|---|---|
| Our Method | point $\mathbf{q}$ + orientation & scale of 2 lines through $\mathbf{q}$ | distance, tangent plane, curvature and $3^{rd}$ order param. at $\mathbf{r}$ |
| [2, 3] | point $\mathbf{q}$ + orientation of 3 lines through $\mathbf{q}$ | distance, tangent plane at $\mathbf{r}$ |

## 2 Setup and Problem Formulation

The geometric setup is depicted in Fig. 1(a). A calibrated scene composed of a pattern of intersecting lines is reflected off an unknown smooth mirror surface and the reflection is observed by a calibrated camera. Our goal is to obtain local geometrical information of the surface by analyzing the deformation produced upon the pattern of lines.

Let $\mathbf{c}$ be the center of projection of the camera. The image plane is positioned $l$ unit distance in front of $\mathbf{c}$, perpendicular to the view direction $\mathbf{v}$. Given a scene point $\mathbf{p}$, let $\mathbf{q}$ be the image of $\mathbf{p}$ observed on the image plane through a specular reflection on the mirror surface at $\mathbf{r}$. See Fig. 2(a). Then $\mathbf{q}$ and $\mathbf{r}$ are constrained by the following relationship:

$$\mathbf{r} = \mathbf{c} + s\,\mathbf{d}, \tag{1}$$

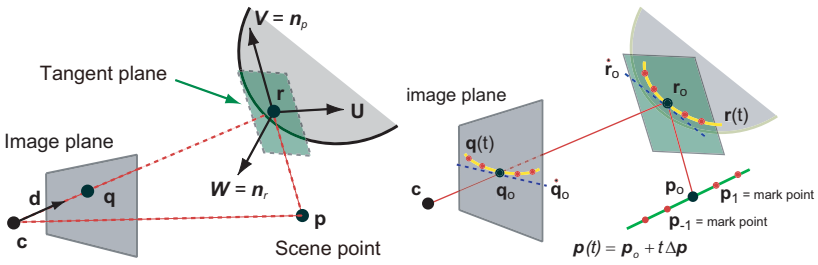


**Fig. 2. Specular reflection geometry**

where the unit vector $\mathbf{d} = (\mathbf{q} - \mathbf{c})/\,||\,\mathbf{q} - \mathbf{c}\,||$ is the view ray direction, and $s = ||\,\mathbf{r} - \mathbf{c}\,||$ is the distance from $\mathbf{r}$ to $\mathbf{c}$. With $\mathbf{c}$ fixed and $\mathbf{q}$ measured, the surface position at $\mathbf{r}$ is completely determined by a single distance parameter $s$.

To recover the higher-order surface parameters around the reflection point $\mathbf{r}$ besides its position, we introduce a suitable coordinate reference system $[\mathbf{U}\,\mathbf{V}\,\mathbf{W}]$ centered at $\mathbf{r}$ and refer to it as the *principal reference system*, similar to that adopted in [5, 2]. Let $\mathbf{n}_p$ be the normal vector to the plane defined by $\mathbf{q}$, $\mathbf{p}$ and $\mathbf{c}$, and let $\mathbf{n}_r$ be the surface normal at $\mathbf{r}$. Then, $\mathbf{W} = \mathbf{n}_r$, $\mathbf{V} = \mathbf{n}_p$, and $\mathbf{U} = \mathbf{V} \times \mathbf{W}$. Given an arbitrary point $\mathbf{x}$ represented in a reference system $[\mathbf{X}\,\mathbf{Y}\,\mathbf{Z}]$ centered in $\mathbf{c}$, its corresponding coordinates $\mathbf{x}'$ in $[\mathbf{U}\,\mathbf{V}\,\mathbf{W}]$ can be obtained by a transformation $\mathbf{x}' = \mathbf{R}^{\mathrm{T}}(\mathbf{x} - \mathbf{r})$, where $\mathbf{R} = [\mathbf{n}_p \times \mathbf{n}_r\, \mathbf{n}_p\, \mathbf{n}_r]$, which is a function of the unknown parameter $s$. In the principal reference system, the normal of the surface at the origin is $\mathbf{W}$ and the tangent plane to the surface is the plane defined by $\mathbf{U}$ and $\mathbf{V}$, thus the surface around $\mathbf{r}$ can be written in the *special Monge form* [8], yielding

$$w = \frac{1}{2!}(a\,u^2 + 2c\,uv + b\,v^2) + \frac{1}{3!}(e\,u^3 + 3f\,u^2v + 3g\,uv^2 + h\,v^3) + \cdots, \quad (2)$$

where we call $a$, $b$, $c$ and $e$, $f$, $g$, $h$ the second-order and third-order surface parameters around $\mathbf{r}$, respectively. Accordingly, we refer to $s$ as the first-order surface parameter which determines both position and normal of the surface. From now on we assume that we work in the local principal reference system.

### 2.1 Surface Recovery

Our focus in this paper is to recover first-, second- and third-order surface parameters around $\mathbf{r}$ using quantities that are known or measurable. Note that $\mathbf{c}$, $\mathbf{q}$, $\mathbf{p}$ are known by assuming calibrated camera and scene.

Consider two lines intersecting at a point $\mathbf{p}$. Through specular reflection, these two lines becomes two curves on the mirror surface intersecting at $\mathbf{r}$ and subsequently are observed as two deformed curves on the image plane, intersecting at $\mathbf{q}$ (the image of $\mathbf{p}$). Our approach is to perform differential analysis

around $\mathbf{q}$. Specifically, we derive analytical expressions for the first- and second-order derivatives of the two deformed image curves at $\mathbf{q}$, in terms of surface parameters up to the third order $(s, a, b, c, e, f, g, h)$ (see Section 3). By comparing these analytical formulas with their corresponding local measurements in the image obtained from scale and orientation of the lines at $\mathbf{q}$ (see Section 5), we impose a set of constraints on the unknown surface parameters. The resulting constraint system leads to solution for $s$ and closed-form solutions of the remaining unknowns, allowing us to recover the mirror surface locally around the reflection point $\mathbf{r}$ up to the third-order accuracy (see Section 4). Our results are summarized in Table 1.

## 3 Differential Analysis

A line passing through a scene point $\mathbf{p}_o(= [\mathbf{p}_{ou}\ \mathbf{p}_{ov}\ \mathbf{p}_{ow}]^{\mathrm{T}})$ in 3D space can be described in a parametric form by $\mathbf{p}(t) = \mathbf{p}_o + t\,\Delta\mathbf{p}$, where $t$ is a parameter and $\Delta\mathbf{p} = [\Delta p_u\ \ \Delta p_v\ \ \Delta p_w]^{\mathrm{T}}$ is the orientation vector of the line. Given a fixed camera position $\mathbf{c}$, a mapping from the parameter $t$ to the corresponding reflection point $\mathbf{r}$ in the mirror surface defines a parameterized space curve $\mathbf{r}(t)$ lying on the mirror surface, which describes the position of the reflection point as $t$ varies. See Fig. 2(b). Consequently, through a perspective projection, $\mathbf{r}(t)$ is mapped to another parameterized curve $\mathbf{q}(t)$ on the image plane. In order to perform differential analysis, we denote the first-order derivatives (tangent vector) of $\mathbf{r}(t)$ and $\mathbf{q}(t)$ respectively by $\dot{\mathbf{r}}$ and $\dot{\mathbf{q}}$, and denote their second-order derivatives respectively by $\ddot{\mathbf{r}}$ and $\ddot{\mathbf{q}}$. They are all functions of $t$. When $t = t_o = 0$, we denote $\mathbf{r}(t_o)$ by $\mathbf{r}_o$, which is the reflection point of $\mathbf{p}_o$ on the mirror surface and can be set as the origin of the principal reference system. Accordingly, the values of $\dot{\mathbf{r}}$, $\dot{\mathbf{q}}$, $\ddot{\mathbf{r}}$ and $\ddot{\mathbf{q}}$ evaluated at $t_o$ are denoted by $\dot{\mathbf{r}}_o$, $\dot{\mathbf{q}}_o$, $\ddot{\mathbf{r}}_o$ and $\ddot{\mathbf{q}}_o$. Throughout this paper, if there is no further explanation, we always assume that we evaluate $\dot{\mathbf{r}}$, $\dot{\mathbf{q}}$, $\ddot{\mathbf{r}}$ and $\ddot{\mathbf{q}}$ at $t_o$, and omit the subscript $o$ to make the notation easier on the eye.

### 3.1 First-order Derivative of $\mathbf{r}(t)$

By formulating a specular reflection path from $\mathbf{p}$ to $\mathbf{q}$ as Chen and Arvo [7] did and carrying out implicit differentiation [2], we can compute $\dot{\mathbf{r}}(= [\dot{u}\,\dot{v}\,\dot{w}]^{\mathrm{T}})$ analytically as

$$\begin{bmatrix} \dot{u} \\ \dot{v} \\ \dot{w} \end{bmatrix} = -\frac{1}{\Delta} \begin{bmatrix} J_v - 2b\cos\theta & 2c\cos\theta & 0 \\ 2c\cos\theta & J_u - 2a\cos\theta & 0 \\ 0 & 0 & \Delta \end{bmatrix} \begin{bmatrix} B_u \\ B_v \\ 0 \end{bmatrix} \tag{3}$$

where $\theta$ is the reflection angle at $\mathbf{r}_o$, and

$$\Delta = (J_u - 2a\cos\theta)(J_v - 2b\cos\theta) - 4c^2\cos^2\theta$$
$$B_v = -\frac{\Delta p_v}{||\,\mathbf{p}_o\,||}; \quad B_u = \frac{\Delta p_w \cos\theta\sin\theta - \Delta p_u\cos^2\theta}{||\,\mathbf{p}_o\,||}$$

$$J_u = J_v \cos^2\theta; \quad J_v = \frac{s + ||\,\mathbf{p}_o\,||}{s\;||\,\mathbf{p}_o\,||} \quad \cos\theta = \frac{\sqrt{2}}{2}\sqrt{\frac{s - \langle \mathbf{d}, \mathbf{p}_o \rangle}{||\,s\mathbf{d} - \mathbf{p}_o\,||} + 1}.$$

Equation (3) holds when $\Delta \neq 0$, which is true in general [2]. With $\mathbf{p}_o$, $\Delta\mathbf{p}$ and $\mathbf{c}$ fixed for a given scene line, Eq. (3) expresses $\dot{\mathbf{r}}$ as a function of unknown surface parameters $s, a, b, c$. A similar equation was derived by Zisserman *et al.* [15] in the dual context of a moving observer.

In [2] we found that if (at least) 2 scene lines $\mathbf{p}_i$, $\mathbf{p}_j$ intersecting at $\mathbf{p}_o$ are available, $a$,$b$,$c$ can be expressed as a function of $s$ and a free parameter $r$:

$$\begin{cases} a = \frac{J_u}{2\cos\theta} - r\frac{h_1}{2\cos\theta} \\ b = \frac{J_v}{2\cos\theta} - r\frac{h_2}{2\cos\theta} \\ c = r\frac{h_3}{2\cos\theta} \end{cases}, \tag{4}$$

where $[h_1 \;\; h_2 \;\; h_3]^{\mathrm{T}} = \mathbf{h}_k \times \mathbf{h}_j$, $\mathbf{h}_i = [B_{v_i}, -B_{u_i}\tan\phi_i, B_{u_i} - B_{v_i}\tan\phi_i]$ and $\phi_i$ denotes the angle between $\dot{\mathbf{r}}_i$ and the $\mathbf{U}$ axis at $\mathbf{r}_o$.

### 3.2 Second-Order Derivative of $\mathbf{r}(t)$

Let $f(u, v, w) = 0$ denote the implicit function of the mirror surface $\mathbf{s}$ represented in Eq. (2) and $\mathbf{H_s} = \partial^2 f / \partial \mathbf{r}^2$ be the Hessian matrix of the function $f$ with respect to the reflection point $\mathbf{r}$. Under the assumption that the third-order terms in the Monge form (2) are negligible, in [3] we exploited the property that $\partial \mathbf{H_s}/\partial \mathbf{r} = 0$ at $t = t_o$, and derived a simplified second-order derivative $\ddot{\mathbf{r}}$ of the curve $\mathbf{r}(t)$. We generalize here this result to the case where $e, f, g, h$ are not negligible and obtain a general expression for the second-order derivative $\ddot{\mathbf{r}}$:

$$\ddot{\mathbf{r}} = \begin{bmatrix} \ddot{u} \\ \ddot{v} \\ \ddot{w} \end{bmatrix} = \begin{bmatrix} \ddot{u}_1 \\ \ddot{v}_1 \\ \ddot{w}_1 \end{bmatrix} + \begin{bmatrix} \ddot{u}_2 \\ \ddot{v}_2 \\ 0 \end{bmatrix} = \ddot{\mathbf{r}}_1 + \ddot{\mathbf{r}}_2. \tag{5}$$

The first term $\ddot{\mathbf{r}}_1$ is given by $\ddot{w}_1 = -a\dot{u}^2 - 2c\dot{u}\dot{v} - b\dot{v}^2$ and

$$\begin{bmatrix} \ddot{u}_1 \\ \ddot{v}_1 \end{bmatrix} = -\frac{1}{\Delta}\begin{bmatrix} J_v - 2b\cos\theta & 2c\cos\theta \\ 2c\cos\theta & J_u - 2a\cos\theta \end{bmatrix}\begin{bmatrix} D_1 - J_w\ddot{w} \\ D_2 \end{bmatrix}, \tag{6}$$

where $J_w = ((||\,\mathbf{p}_o\,|| - s)\sin\theta\cos\theta)\,/(s\,||\,\mathbf{p}_o\,||)$, and $D_1, D_2$ are functions depending only on $s, a, b, c$. The second term $\ddot{\mathbf{r}}_2$ depends on the third-order surface parameters and is expressed as:

$$\begin{bmatrix} \ddot{u}_2 \\ \ddot{v}_2 \end{bmatrix} = \frac{2\cos\theta}{\Delta}\begin{bmatrix} J_v - 2b\cos\theta & 2c\cos\theta \\ 2c\cos\theta & J_u - 2a\cos\theta \end{bmatrix}\begin{bmatrix} \dot{u}^2 & 2\dot{u}\dot{v} & \dot{v}^2 & 0 \\ 0 & \dot{u}^2 & 2\dot{u}\dot{v} & \dot{v}^2 \end{bmatrix}\begin{bmatrix} e \\ f \\ g \\ h \end{bmatrix}. \tag{7}$$

Detailed derivation of Eq. (6) and Eq. (7) is available as a technical report.

### 3.3 Relationship between $\dot{\mathbf{r}}$ and $\dot{\mathbf{q}}$

Based on Eq. (3), we derive an analytical formula for the first-order derivative of $\mathbf{q}(t)$ on the image plane by examining the relationship between $\dot{\mathbf{r}}$ and $\dot{\mathbf{q}}$.

Letting $\lambda(t) = ||\,\mathbf{q}(t) - \mathbf{c}\,|| \,/\, ||\,\mathbf{r}(t) - \mathbf{c}\,||$ be the ratio between the distance from $\mathbf{c}$ to $\mathbf{q}(t)$ and that from $\mathbf{c}$ to $\mathbf{r}(t)$. We may express the image plane curve $\mathbf{q}(t)$ as follows:

$$\mathbf{q}(t) - \mathbf{c} \;=\; \lambda(t)(\mathbf{r}(t) - \mathbf{c}). \tag{8}$$

In our setup the image plane is located $l$ unit distance along the view direction $\mathbf{v}$, thus $\lambda$ satisfies the following equation

$$\lambda(t)\,\langle \mathbf{r}(t) - \mathbf{c}, \mathbf{v}\rangle \;=\; l. \tag{9}$$

Here, $\langle\,,\rangle$ denotes the inner product of two vectors. Using Eq. (9), we may evaluate $\lambda$ and $\dot{\lambda}$ at $t_o$ as

$$\lambda \;=\; \frac{l}{s\,\langle \mathbf{d}, \mathbf{v}\rangle}, \qquad \dot{\lambda} \;=\; -\frac{l\,\langle \dot{\mathbf{r}}, \mathbf{v}\rangle}{s^2\,\langle \mathbf{d}, \mathbf{v}\rangle^2}. \tag{10}$$

Then we can differentiate Eq. (8) with respect to $t$ and compute $\dot{\mathbf{q}}$ as follows:

$$\dot{\mathbf{q}} \;=\; \lambda\dot{\mathbf{r}} + s\dot{\lambda}\mathbf{d} \;=\; \frac{l}{s\,\langle \mathbf{d}, \mathbf{v}\rangle}\left[\mathbf{I} - \frac{\mathbf{d}\mathbf{v}^{\mathrm{T}}}{\langle \mathbf{d}, \mathbf{v}\rangle}\right]\dot{\mathbf{r}} \;=\; \mathbf{T}\,\dot{\mathbf{r}}, \tag{11}$$

where the $3 \times 3$ matrix $\mathbf{T}$ is defined as

$$\mathbf{T} \;=\; \frac{l}{s\,\langle \mathbf{d}, \mathbf{v}\rangle}\left[\mathbf{I} - \frac{\mathbf{d}\mathbf{v}^{\mathrm{T}}}{\langle \mathbf{d}, \mathbf{v}\rangle}\right]. \tag{12}$$

### 3.4 Relationship between $\ddot{\mathbf{q}}$ and $\ddot{\mathbf{r}}$, $\dot{\mathbf{r}}$

To relate the second-order derivative of $\mathbf{r}(t)$ to that of its image plane projection $\mathbf{q}(t)$, we differentiate Eq. (11) with respect to $t$, obtaining

$$\lambda\ddot{\mathbf{q}} \;=\; \lambda^2\ddot{\mathbf{r}} + (\ddot{\lambda}\lambda - 2\dot{\lambda}^2)s\,\mathbf{d} + 2\dot{\lambda}\dot{\mathbf{q}}, \tag{13}$$

where $\lambda$ and $\dot{\lambda}$ are defined in Eq. (10). By differentiating Eq. (9) twice with respect to $t$, we can compute $\ddot{\lambda}$ and then get an analytical formula for $\ddot{\mathbf{q}}$ from Eq. (13), that is

$$\ddot{\mathbf{q}} = \mathbf{T}\left[\ddot{\mathbf{r}} - \frac{2}{s\,\langle \mathbf{d}, \mathbf{v}\rangle}\,\langle \dot{\mathbf{r}}, \mathbf{v}\rangle\,\dot{\mathbf{r}}\right], \tag{14}$$

where the matrix $\mathbf{T}$ is defined as in Eq. (12). It then follows from Eq. (5) that $\ddot{\mathbf{q}} = \ddot{\mathbf{q}}_1 + \ddot{\mathbf{q}}_2$, where

$$\ddot{\mathbf{q}}_1 = \mathbf{T}\left[\ddot{\mathbf{r}}_1 - \frac{2}{s\,\langle \mathbf{d}, \mathbf{v}\rangle}\,\langle \dot{\mathbf{r}}, \mathbf{v}\rangle\,\dot{\mathbf{r}}\right], \quad \ddot{\mathbf{q}}_2 = \mathbf{T}\,\ddot{\mathbf{r}}_2. \tag{15}$$

As we can see, the third-order surface parameters $e, f, g, h$ only appear in $\ddot{\mathbf{q}}_2$.

## 4 Surface Reconstruction

In this section we shall show that by using *two* scene lines intersecting at a point $\mathbf{p}_o$, we are able to recover first order surface parameter $s$ and higher order parameters $a, b, c, e, f, g, h$ in close form using Eq. (11) and Eq. (15). For clarity, we indicate the quantities measured in the image plane with the superscript $m$ and the quantities associated with different scene lines with a subscript. For example, the measurement of the first-order derivative of the $i$th curve $\mathbf{q}_i(t)$ in the image plane is indicated by $\dot{\mathbf{q}}_i^m$.

### 4.1 Recovering First and Second Order Parameters

It can be seen from Eq. (4) that we only need to determine two unknowns $r$ and $s$ to recover first and second-order surface parameters. Replacing $a, b, c$ in Eq. (3) by Eq. (4), we obtain a novel expression for $\dot{\mathbf{r}}$ in terms of $r$ and $s$ (embedded in $h_1, h_2, h_3, B_u, B_v$) as:

$$\dot{\mathbf{r}} = -\frac{1}{r(h_1h_2 - h_3^2)} \begin{bmatrix} h_2 & h_3 & 0 \\ h_3 & h_1 & 0 \\ 0 & 0 & r(h_1h_2 - h_3^2) \end{bmatrix} \begin{bmatrix} B_u \\ B_v \\ 0 \end{bmatrix} = -\frac{1}{r} \begin{bmatrix} \mathbf{V}\,\mathbf{B} \\ 0 \end{bmatrix},$$

where we have defined

$$\mathbf{V} \;=\; \frac{1}{h_1h_2 - h_3^2} \begin{bmatrix} h_2 & h_3 \\ h_3 & h_1 \end{bmatrix}, \quad \mathbf{B} \;=\; \begin{bmatrix} B_u \\ B_v \end{bmatrix}.$$

Accordingly, it follows from Eq. (11) that the first-order derivative $\dot{\mathbf{q}}$ and its $L_2$ norm can also be expressed in terms of the two unknowns $r$ and $s$:

$$\dot{\mathbf{q}} \;=\; -\frac{1}{r}\mathbf{T} \begin{bmatrix} \mathbf{V}\,\mathbf{B} \\ 0 \end{bmatrix}, \quad ||\,\dot{\mathbf{q}}\,||^2 \;=\; \langle \dot{\mathbf{q}}, \dot{\mathbf{q}} \rangle \;=\; \frac{1}{r^2} \begin{bmatrix} \mathbf{B}^{\mathrm{T}}\mathbf{V}^{\mathrm{T}}\, 0 \end{bmatrix} \mathbf{T}^{\mathrm{T}}\mathbf{T} \begin{bmatrix} \mathbf{V}\mathbf{B} \\ 0 \end{bmatrix} \quad (16)$$

where only the unknown $s$ (not $r$) appears in $\mathbf{T}$, $\mathbf{V}$ and $\mathbf{B}$.

Suppose that we are able to measure tangent directions ($\tan\phi_k$ and $\tan\phi_j$) and first-order derivatives ($\dot{\mathbf{q}}_k^m$ and $\dot{\mathbf{q}}_j^m$) of $\mathbf{q}_k(t)$ and $\mathbf{q}_j(t)$ at $\mathbf{q}_o$, respectively (see Section 5). By taking the ratio $||\,\dot{\mathbf{q}}_k^m\,||^2 \,/\, \left|\left|\,\dot{\mathbf{q}}_j^m\,\right|\right|^2$, we have

$$\frac{||\,\dot{\mathbf{q}}_k^m\,||^2}{\left|\left|\,\dot{\mathbf{q}}_j^m\,\right|\right|^2} \;=\; \frac{\begin{bmatrix} \mathbf{B}_k{}^{\mathrm{T}}\mathbf{V}^{\mathrm{T}}\, 0 \end{bmatrix} \mathbf{T}^{\mathrm{T}}\mathbf{T} \begin{bmatrix} \mathbf{V}\mathbf{B}_k \\ 0 \end{bmatrix}}{\begin{bmatrix} \mathbf{B}_j{}^{\mathrm{T}}\mathbf{V}^{\mathrm{T}}\, 0 \end{bmatrix} \mathbf{T}^{\mathrm{T}}\mathbf{T} \begin{bmatrix} \mathbf{V}\mathbf{B}_j \\ 0 \end{bmatrix}}, \quad (17)$$

where the matrix $\mathbf{V}$ is expressed in terms of our tangent direction measurements $\tan\phi_k$ and $\tan\phi_j$. Notice that the matrix $\mathbf{T}$ defined in Eq. (12) does not depend on a particular line. Equation (17) imposes a constraint for us to solve for $s$. Once $s$ is computed, we can easily derive the closed-form solution for another unknown $r$ up to a sign from Eq. (16):

$$r^2 \;=\; \frac{\begin{bmatrix} \mathbf{B}_k{}^{\mathrm{T}}\mathbf{V}^{\mathrm{T}}\, 0 \end{bmatrix} \mathbf{T}^{\mathrm{T}}\mathbf{T} \begin{bmatrix} \mathbf{V}\mathbf{B}_k \\ 0 \end{bmatrix}}{||\,\dot{\mathbf{q}}_k^m\,||^2}. \quad (18)$$

### 4.2 Recovering Third Order Parameters

To recover the third-order surface parameters, we assume that we are able to estimate the second-order derivatives for the two reflection curves in the image plane, denoted by $\ddot{\mathbf{q}}_k^m$ and $\ddot{\mathbf{q}}_j^m$ respectively (see Section 5). Let $\hat{\mathbf{v}}$ denote a 2D vector consisting of the first two components of a 3D vector $\mathbf{v}$. In accordance with the decomposition of $\ddot{\mathbf{q}}$ in Eq. (15), we can divide $\hat{\ddot{\mathbf{q}}}_k^m$ and $\hat{\ddot{\mathbf{q}}}_j^m$ into two parts, yielding:

$$(\hat{\ddot{\mathbf{q}}}_2)_k^m \;=\; \hat{\ddot{\mathbf{q}}}_k^m - (\hat{\ddot{\mathbf{q}}}_1)_k, \quad (\hat{\ddot{\mathbf{q}}}_2)_j^m \;=\; \hat{\ddot{\mathbf{q}}}_j^m - (\hat{\ddot{\mathbf{q}}}_1)_j, \tag{19}$$

where $(\hat{\ddot{\mathbf{q}}}_1)_k$ and $(\hat{\ddot{\mathbf{q}}}_1)_j$ (independent of $e, f, g, h$) are known from Eq. (6) once we have recovered $s, a, b, c$. On the other hand, we have analytical solutions for $(\hat{\ddot{\mathbf{q}}}_2)_k$ and $(\hat{\ddot{\mathbf{q}}}_2)_j$ from Eq. (15), that is,

$$(\hat{\ddot{\mathbf{q}}}_2)_k = \mathbf{T}_{22}(\hat{\ddot{\mathbf{r}}}_2)_k, \quad (\hat{\ddot{\mathbf{q}}}_2)_j = \mathbf{T}_{22}(\hat{\ddot{\mathbf{r}}}_2)_j, \tag{20}$$

where $\mathbf{T}_{22}$ is the upper left $2 \times 2$ sub-matrix of $\mathbf{T}$, and $\hat{\ddot{\mathbf{r}}}_2$ can be expressed from Eq. (7) using Eq. (4) as

$$\begin{bmatrix} \ddot{u}_2 \\ \ddot{v}_2 \end{bmatrix} = \frac{2\cos\theta}{r(h_1h_2 - h_3^2)} \begin{bmatrix} h_2 & h_3 \\ h_3 & h_1 \end{bmatrix} \begin{bmatrix} \dot{u}^2 & 2\dot{u}\dot{v} & \dot{v}^2 & 0 \\ 0 & \dot{u}^2 & 2\dot{u}\dot{v} & \dot{v}^2 \end{bmatrix} \begin{bmatrix} e \\ f \\ g \\ h \end{bmatrix}. \tag{21}$$

Thus, Equating Eq. (19) and Eq. (20) gives rise to a constraint system for $e, f, g, h$:

$$\begin{bmatrix} (\hat{\ddot{\mathbf{q}}})_k^m - (\hat{\ddot{\mathbf{q}}}_1)_k \\ (\hat{\ddot{\mathbf{q}}})_j^m - (\hat{\ddot{\mathbf{q}}}_1)_j \end{bmatrix} \;=\; \frac{2\cos\theta}{r(h_1h_2 - h_3^2)} \mathbf{M}_1\mathbf{M}_2\mathbf{M}_3 \begin{bmatrix} e \\ f \\ g \\ h \end{bmatrix}, \tag{22}$$

where $\mathbf{M}_1, \mathbf{M}_2, \mathbf{M}_3$ are defined as follows:

$$\mathbf{M}_1 = \begin{bmatrix} h_2 & h_3 & 0 & 0 \\ h_3 & h_1 & 0 & 0 \\ 0 & 0 & h_2 & h_3 \\ 0 & 0 & h_3 & h_1 \end{bmatrix}, \; \mathbf{M}_2 \;=\; \begin{bmatrix} \mathbf{T}_{22} & \mathbf{0} \\ \mathbf{0} & \mathbf{T}_{22} \end{bmatrix}, \; \mathbf{M}_3 = \begin{bmatrix} \dot{u}_k^2 & 2\dot{u}_k\dot{v}_k & \dot{v}_k^2 & 0 \\ 0 & \dot{u}_k^2 & 2\dot{u}_k\dot{v}_k & \dot{v}_k^2 \\ \dot{u}_j^2 & 2\dot{u}_j\dot{v}_j & \dot{v}_j^2 & 0 \\ 0 & \dot{u}_j^2 & 2\dot{u}_j\dot{v}_j & \dot{v}_j^2 \end{bmatrix} \tag{23}$$

Equation (22) leads to the following closed-form solution for the third-order surface parameters, that is,

$$\begin{bmatrix} e \\ f \\ g \\ h \end{bmatrix} \;=\; \frac{r(h_1h_2 - h_3^2)}{2\cos\theta} (\mathbf{M}_1\mathbf{M}_2\mathbf{M}_3)^{-1} \begin{bmatrix} (\hat{\ddot{\mathbf{q}}})_k^m - (\hat{\ddot{\mathbf{q}}}_1)_k \\ (\hat{\ddot{\mathbf{q}}})_j^m - (\hat{\ddot{\mathbf{q}}}_1)_j \end{bmatrix}, \tag{24}$$

where the existence of $(\mathbf{M}_1\mathbf{M}_2\mathbf{M}_3)^{-1}$ is based on the following proposition:

**Proposition 1** The matrix $\mathbf{M}_1\mathbf{M}_2\mathbf{M}_3$ is invertible.

**Proof:** $\det(\mathbf{M}_1) \neq 0$ follows directly from $\Delta \neq 0$. It can be easily proved that $\det(\mathbf{M}_2) \neq 0$ since $\mathbf{T}$ in Eq. (11) is associated with the projective transformation from a mirror surface (3 D.O.F.) into the image plane (2 D.O.F.). Let us prove that $\det(\mathbf{M}_3) \neq 0$. We first show that $\mathbf{M}_3$ is invertible when one of $\{\dot{u}_k, \dot{v}_k, \dot{u}_j, \dot{v}_j\}$ is zero. For example, if $\dot{u}_k = 0$, then $\det(\mathbf{M}_3) = (\dot{v}_k\dot{u}_j)^4 \neq 0$. Otherwise, either $\dot{v}_k = 0$ or $\dot{u}_j = 0$ will contradict to our observation of two curves with different orientations. Next we shall consider the case where none of $\dot{u}_k, \dot{v}_k, \dot{u}_j, \dot{v}_j$ is zero. The proof is performed by contradiction. With two differently-oriented image curves observed, we should have

$$\dot{v}_k/\dot{u}_k \neq \dot{v}_j/\dot{u}_j, \quad \dot{v}_k/\dot{u}_k \neq -\dot{v}_j/\dot{u}_j. \tag{25}$$

Suppose that $\mathbf{M}_3$ is singular. Its 4 row vectors $U_1, U_2, U_3, U_4$ are linearly dependent. Without loss of generality, we may assume that $U_4 = k_1U_1 + k_2U_2 + k_3U_3$ (at least one $k_i$ is nonzero), which can be expanded as

$$k_1\dot{u}_k^2 + k_3\dot{u}_j^2 = 0 \tag{26}$$

$$2k_1\dot{u}_k\dot{v}_k + k_2\dot{u}_k^2 + 2\,k_3\dot{u}_j\dot{v}_j = \dot{u}_j^2 \tag{27}$$

$$k_1\dot{v}_k^2 + 2\,k_2\dot{u}_k\dot{v}_k + k_3\dot{v}_j^2 = 2\dot{u}_j\dot{v}_j \tag{28}$$

$$k_2\dot{v}_k^2 = \dot{v}_j^2 \tag{29}$$

By eliminating variables through substitutions, we get

$$(k_1 + k_2k_3)(k_3\dot{v}_k + \dot{u}_k)^2 = 0, \quad (k_1 + k_2k_3)(k_1\dot{v}_j - k_2\dot{u}_j)^2 = 0. \tag{30}$$

If $k_1+k_2k_3 = 0$, then it follows from Eqs. (26) and (29) that $k_3\left[\dot{v}_j^2/\dot{v}_k^2 - \dot{u}_j^2/\dot{u}_k^2\right] = 0$. To satisfy Eq. (25), we must have $k_3 = 0$, which leads to $k_1 = 0$ and then $\dot{v}_k/\dot{u}_k = \dot{v}_j/\dot{u}_j$ from Eqs. (27) and (28), contradictory to our assumption (25). Consequently, Equation (30) simplifies to

$$k_3\dot{v}_k + \dot{u}_k = 0, \quad k_1\dot{v}_j - k_2\dot{u}_j = 0. \tag{31}$$

Eqs. (31), (26) and (29) present an over-constrained system for $k_1, k_2, k_3$, which requires $\dot{v}_k/\dot{u}_k = \dot{v}_j/\dot{u}_j$, again contradictory to our assumption (25). Therefore, $U_1$, $U_2$, $U_3$, $U_4$ must be linearly independent, and $\mathbf{M}_3$ is invertible. □□

## 5 Numerical Measurement and Error Analysis

In Section 4 we have assumed that for a reflected curve $\mathbf{q}(t)$ observed on the image plane, we are able to measure its orientation $\tan\phi$, the first-order derivative $\dot{\mathbf{q}}^m$ and the second-order derivative $\ddot{\mathbf{q}}^m$ at $\mathbf{q}_o$. In this section we shall describe

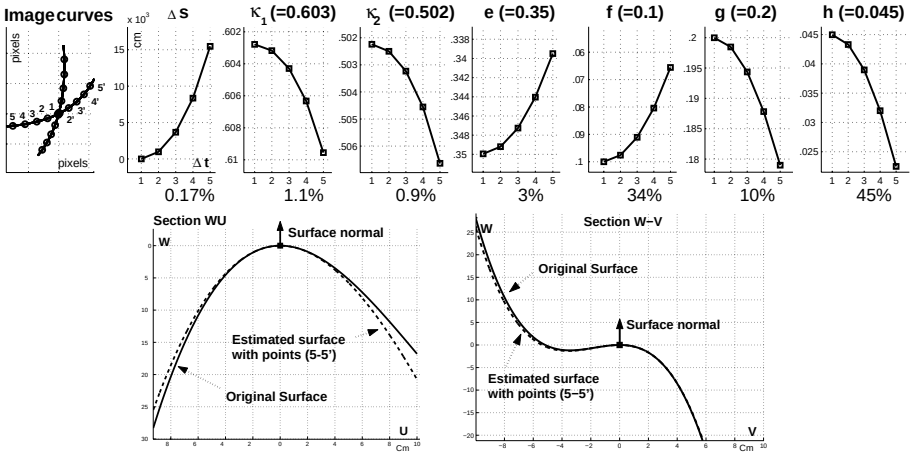


**Fig. 3. Reconstruction error analysis by means of numerical simulations on a synthetic mirror surface**. Given the center of the camera $\mathbf{c}$ and 2 scene lines intersecting at $\mathbf{p}_o$, we observe two reflected image curves depicted in the top left panel. The synthetic mirror surface is positioned such that the distance $s$ between the reflecting point $\mathbf{r}_o$ and $\mathbf{c}$ is 9cm. The surface principal curvatures at $\mathbf{r}_o$ are $\kappa_1 = -0.603$ and $\kappa_2 = -0.502$, and the third-order surface parameters are $e = -0.35, f = -0.1, g = 0.2, h = -0.045$. By numerically measuring the first- and second-order derivatives at $\mathbf{q}_o$ (i.e. point 1) using pairs of mark points located at increasing distance $\Delta t$ from $\mathbf{q}$ (i.e. mark point pair $(2, 2'), \cdots (5, 5')$), we recover the local surface at $\mathbf{r}_o$ as described in Section 4. Each of the remaining plots in the top panel recovered surface parameter as a function of the mark gap $\Delta t$, with the maximum percentage error reported at the bottom. Notice that the error of recovered distance $s$ increases as a quadratic function of $\Delta t$, the curvature error is one order of magnitude bigger than the distance error, and the third-order parameter error is one order of magnitude bigger than the curvature error. In the bottom panels the reconstructed surface (estimated by using the pair of mark points $(5, 5')$) is qualitatively compared to the original one in both $\mathbf{W}-\mathbf{V}$ and $\mathbf{W}-\mathbf{U}$ sections of the $\mathbf{UVW}$ reference system. The numerical approximation (32) and (33) appears to give rise to reasonably good reconstruction results as long as the mark points are close enough to each other (i.e., $\Delta t$ small enough).

how to numerically compute these quantities, and analyze the reconstruction error due to such approximations.

Given a scene line $\mathbf{p}(t)$, we may accurately measure the orientation of its reflected image curve $\mathbf{q}(t)$ at $\mathbf{q}_o$ using B-spline interpolation. In fact, by constructing a B-spline that interpolates image points along the curve, the direction of $\dot{\mathbf{q}}$ (i.e.,$\tan\phi$) can be calculated by numerical differentiation of the resulting B-spline. To estimate a complete $\dot{\mathbf{q}}$ (with both direction and magnitude) and higher-order derivative $\ddot{\mathbf{q}}$, we can make use of mark points $\mathbf{p}_o = \mathbf{p}(t_o), \mathbf{p}_{-1} = \mathbf{p}(t_{-1}), \mathbf{p}_1 = \mathbf{p}(t_1), \ldots$ (see Fig. 2) distributed along $\mathbf{p}(t)$ and use central finite difference approximation. Specifically, suppose that the mark points

$\mathbf{p}(t_i)(i = \ldots, -1, 0, 1, \ldots)$ are mapped to corresponding image points $\mathbf{q}(t_i)$. Let the step size $\Delta t = t_i - t_{i-1}$. We may approximate $\dot{\mathbf{q}}$ and $\ddot{\mathbf{q}}$ at $\mathbf{q}_o$ by using 2 points and 3 points respectively, that is

$$\dot{\mathbf{q}} \approx (\mathbf{q}(t_1) - \mathbf{q}(t_{-1}))/(2\Delta t) \tag{32}$$

$$\ddot{\mathbf{q}} \approx (\mathbf{q}(t_1) - 2\mathbf{q}(t_0) + \mathbf{q}(t_{-1}))/(\Delta t)^2. \tag{33}$$

The truncation error of the finite difference approximation (32) and (33) decays when $\Delta t$ decreases. To analyze how this numerical approximation affects recovery of distance, curvature and third-order parameters of the mirror surface, we conducted numerical simulations on a synthetic mirror surface by implementing Eqs. (17), (18) and (24) in Matlab (see Fig. 3).

## 6 Experimental Results

In addition to numerical simulations on synthetic surfaces, we also validated our theoretical results by recovering local surface parameters of some real mirror objects. A Kodak DC290 digital camera with $1792 \times 1200$ resolution was used to take a picture of a mirror surface reflecting a checkerboard pattern of 2cm $\times$ 2cm grid size. The mirror surface and camera were set about 30cm apart. The edges of the pattern grids acted as a pair of intersecting lines and corners served as mark points for our finite difference approximation. The pattern was placed such that both pattern and its specular reflection were clearly visible from the camera (see Fig. 1). The camera and pattern were calibrated using standard calibration routines. Our local surface reconstruction algorithm can be summarized as the following 8 steps:

1. Select a scene intersection point and its reflected point (e.g. 1 and $1'$ in Fig. 1).
2. Select four neighboring points from both checkerboard pattern (e.g. 2, 3, 4, 5) and corresponding reflected pattern (e.g. $2'$, $3'$, $4'$, $5'$).
3. From 1, 2, 3, 4, 5 compute $\mathbf{p}_o$ and the direction of two scene lines $\Delta\mathbf{p}_1$ and $\Delta\mathbf{p}_2$.
4. From $1'$, $2'$, $3'$, $4'$, $5'$ estimate $\mathbf{q}^m$, $\dot{\mathbf{q}}_1^m$, $\dot{\mathbf{q}}_2^m$ and $\ddot{\mathbf{q}}_1^m$, $\ddot{\mathbf{q}}_2^m$ using Eqs. (32) and (33).
5. Recover the distance parameter $s$ by Eq. (17) from $\dot{\mathbf{q}}_1^m$, $\dot{\mathbf{q}}_2^m$.
6. Recover the parameter $r$ by Eq. (18) from $\dot{\mathbf{q}}_1^m$, $\dot{\mathbf{q}}_2^m$.
7. Recover curvature parameters ($a$, $b$, $c$) by Eq. (4).
8. Recover third-order surface parameters ($e$, $f$, $g$, $h$) by Eq. (24) from $\ddot{\mathbf{q}}_1^m$, $\ddot{\mathbf{q}}_2^m$.

We validated this algorithm with a specular teapot and a portion of car fender (see Fig. 5). The recovery of third-order surface parameters has been validated in Fig. 3 (bottom panel) using a synthetic mirror surface. In the teapot experiments we compared our reconstruction results with those obtained using three lines [2] in Fig. 4.

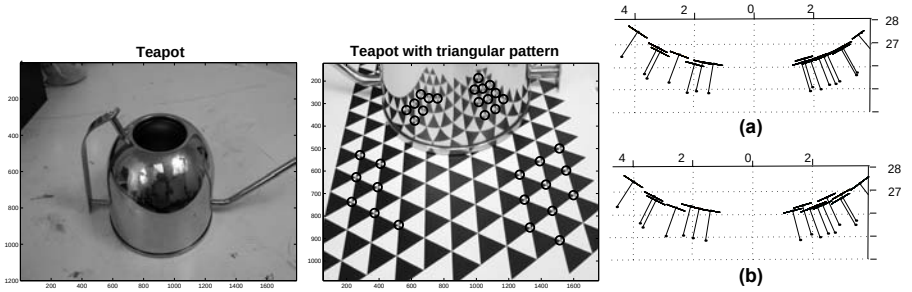


**Fig. 4. Teapot Experiment**. We compared our reconstruction results with those obtained using the 3-lines-approach [2] for a specular teapot (left panel). At that end, we used a special pattern composed of a tessellation of triangles in order to have a triplet of intersecting lines at each corner point. The bottom part of the teapot (a cylinder of diameter $d = 13.15$ cm) was reconstructed at each marked point (middle panel). The right panel compares reconstructed points obtained by 3-lines-method (a) and our method (b). Each point is represented by its tangent plane and its normal vector. Statistical analysis shows that these two methods exhibit similar performances in reconstructing position and surface normal at each intersecting point. Our approach, however, is more advantageous than the 3-lines-approach in that it can also estimate curvature parameters. Our recovered average principal curvatures are $\kappa_1 = -0.153 \pm 0.005$ and $\kappa_2 = 0.003 \pm 0.007$, which corresponds to an average estimated cylinder diameter of 13.097 cm.

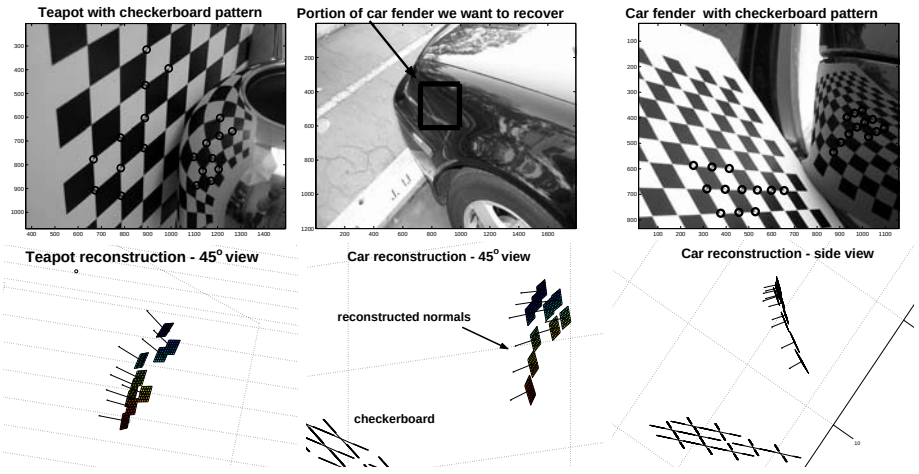


**Fig. 5. Experimental results with real surfaces (teapot and car fender)**.

## 7 Conclusions

Under the assumption of an unknown mirror surface reflecting a known calibrated pattern (e.g. a checkerboard) onto the image plane of a calibrated camera, we demonstrated that surface position and shape up to third order can be

derived as a function of local position, orientation and local scale measurements in the image when two orientations are available at the same point of the image reflected pattern (e.g. a corner). We validated our theoretical results with both numerical simulations and experiments with real surfaces and found that the method is practical and yields good quality surface reconstruction. Future work may be done to overcome the correspondence problem between pattern points and their reflected image points. Additional work may be also needed to remove the hypothesis of having a calibrated pattern, which will most likely require integrating additional cues (such as stereo views) and some form of prior knowledge on the likely statistics of the scene geometry.

## References

1. S. Savarese and P. Perona: Local Analysis for 3D Reconstruction of Specular Surfaces. *IEEE Conf. on Computer Vision and Pattern Recognition*, II 738–745 (2001) *CVPR*, II 738–745 (2001).
2. S. Savarese and P. Perona: Local Analysis for 3D Reconstruction of Specular Surfaces - Part ii. *ECCV*, II 759–774 (2002).
3. S. Savarese, M. Chen, P. Perona: Second Order Local Analysis for 3D Reconstruction of Specular Surfaces. *3DPVT*, 356–360 (2002).
4. T. Binford: Inferring surfaces from images. *Artificial Intelligence*, **17** (1981) 205–244.
5. A. Blake: Specular stereo. *IJCAI* (1985) 973–976.
6. A. Blake and G. Brelstaff: Geometry from specularities. *ICCV Proc. of Int Conf. of Computer Vision* (1988) 394–403.
7. M. Chen and J. Arvo: Theory and Application of Specular Path Perturbation. *ACM Transactions on Graphics*. **19** (2000) 246–278.
8. R. Cipolla and P. Giblin: Visual motion of curves and surfaces. *Cambridge University Press* 2000.
9. M. Halsead, A. Barsky, S. Klein, and R. Mandell: Reconstructing curved surfaces from reflection patterns using spline surface fitting normals. *SIGGRAPH* (1996).
10. G. Healey and T. Binford: Local shape from specularity. *Computer Vision, Graphics, and Image Processing* **42** (1988) 62–86.
11. K. Ikeuchi: Determining surface orientation of specular surfaces by using the photometric stereo method. *IEEE PAMI* **3** (1981) 661–669.
12. J. Koenderink and A. van Doorn: Photometric invariants related to solid shape. *Optica Apta* **27** (1980) 981–996.
13. M. Oren and S. K.Nayar: A theory of specular surface geometry. *Trans. Int. Journal of Computer Vision* (1997) 105–124.
14. J. Zheng and A. Murata: Acquiring a complete 3d model from specular motion under the illumination of circular-shaped light sources. *IEEE PAMI* **8** (2000).
15. A. Zisserman, P. Giblin, and A. Blake: The information available to a moving observer from specularities.*Image and Video Computing* **7** (1989) 38–42.
16. D. Perard: Automated visual inspection of specular surfaces with structured-lighting reflection techniques. *PhD Thesis – VDI Verlag* **Nr. 869** (2001).
17. M. Tarini, H. Lensch, M. Goesele and H.P. Seidel: Shape from Distortion 3D Range Scanning of Mirroring Objects. *Proc. of SIGGRAPH, Sketches and Applications* (2002) 248
18. T. Bonfort and P. Sturm: Voxel Carving for Specular Surfaces. *Proceedings of the 9th IEEE International Conference on Computer Vision* (2003)